Chemical Engineering Science 102 (2013) 151–162

Contents lists available at ScienceDirect

Chemical Engineering Science

journal homepage: www.elsevier.com/locate/ces

Achieving ultra-high platinum utilization via optimization of PEM fuel cell cathode catalyst layer microstructure

J. Marquis [a], M.-O. Coppens [a,b,*]

[a] Isermann Department of Chemical & Biological Engineering, Rensselaer Polytechnic Institute, 110 8th St., Troy, NY, United States
[b] Department of Chemical Engineering, University College London (UCL), Torrington Place, London WC1E 7JE, United Kingdom

GRAPHICAL ABSTRACT

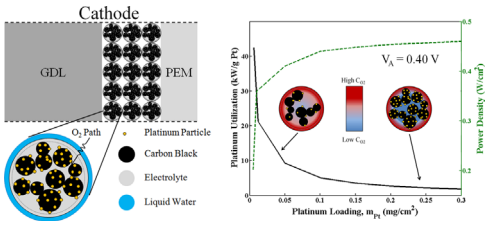

ARTICLE INFO

Article history:
Received 20 December 2012
Received in revised form
31 July 2013
Accepted 4 August 2013
Available online 9 August 2013

Keywords:
Catalysis
Electrochemistry
Energy
Optimization
Fuel cell
Microstructure

ABSTRACT

Inefficient usage of expensive platinum catalyst has plagued the design of PEM fuel cells and contributed to the limited production and use of fuel cell systems. Here, it is shown that hierarchical optimization can increase platinum utilization 30-fold over existing catalyst layer designs while maintaining power densities over 0.35 W/cm^2. The cathode catalyst layer microstructure is optimized with respect to platinum utilization (measured as kilowatts of electricity produced per gram of platinum). A one-dimensional agglomerate model that accounts for liquid water saturation is used in this study. The cathode catalyst layer microstructure is optimized by manipulating the platinum loading (m_{Pt}), platinum-to-carbon ratio (Pt/C), and catalyst layer void fraction (ε_V^{cl}). The resulting catalyst layer microstructure features ultra-low platinum loadings of roughly 0.01 mg/cm^2.

1. Introduction

Global energy demands are projected to increase 50% over current levels by the year 2030 (BP Global, 2011). PEM fuel cells are amongst the most popular candidates for reliably and efficiently converting hydrogen, produced from fossil or renewable sources, into electric power. However, the large-scale implementation of fuel cell technology for use in commercial, residential or transportation applications is hindered largely by the high cost associated with the platinum catalyst (James and Kalinoski, 2009).

PEM fuel cells convert chemical energy to electrical energy by the electrochemical reaction between hydrogen and oxygen. The electrochemical potential of this reaction is approximately 1.23 V. Of particular interest is the oxygen reduction reaction taking place within the cathode catalyst layer.

$$H_2(g) \rightarrow 2H^+ + 2e^- \quad \text{(Anode)}$$

$$\frac{1}{2}O_2(g) + 2H^+ + 2e^- \rightarrow H_2O(l) \quad \text{(Cathode)}$$

Existing fuel cell catalyst layer microstructures are sub-optimally designed, leading to significant transport limitations that result in

* Corresponding author at: Department of Chemical Engineering, University College London (UCL), Torrington Place, London WC1E 7JE, United Kingdom. Tel.: +44 20 3108 1126/7679 3824; fax: +44 20 7383 2348.
E-mail address: m.coppens@ucl.ac.uk (M.-O. Coppens).

0009-2509/$ - see front matter © 2013 Elsevier Ltd. All rights reserved.
http://dx.doi.org/10.1016/j.ces.2013.08.003

inefficient catalyst usage. These considerations have led the US Department of Energy (DOE) to set a target for the total platinum utilization, measured as kilowatts of power produced per gram of platinum. Spendelow et al. (2010) report a target of 8.0 kW/g by 2015 with the best-reported platinum utilization to date being 3.57 kW/g.

The inefficiencies in the cathode catalyst layer stem from several phenomena. These include severe diffusion limitations within catalyst agglomerates, water management within the cathode, and Ohmic loses related to ionic transport. A complete understanding of the issues associated with the cathode catalyst layer begins with a physical description of the domain.

The most common PEM fuel cell microstructure consists of platinum catalyst supported on “carbon black” and coated with electrolyte. The relative amounts of each component in the catalyst layer are determined by the composition of the precursor catalyst ink solution. This solution is typically spray-coated onto the gas diffusion layer or membrane to form the catalyst layer. Soboleva et al. (2010, 2011) conducted nitrogen adsorption experiments to determine the effects of the carbon support, ionomer and platinum loading on the catalyst layer microstructure. Both Ketjen Black and Vulcan XC-72 carbon supports were studied. Ketjen Black differs from Vulcan XC-72 in that it has a larger fraction of micropores (<2 nm). For these two carbon supports it was found that the electrolyte covered pores of <20 nm, effectively blocking reaction sites from the gas phase reactant.

Numerical modeling of such catalyst layers has been widely researched over the past decade. Numerous models with varying degrees of resolution have emerged to capture the complex interactions found in the cathode catalyst layer, including models by Broka and Ekdunge (1997), Marr and Li (1999), Lin et al. (2004), Wang and Nguyen (2008) and many others. Agglomerate models were first introduced in the 1980s by Bernardi and Verbrugge (1991), Iszkowski and Cutlip (1980). A common element in these models is that the carbon-black supported platinum particles aggregate and become encased in electrolyte to form spherical catalyst pellets. This assumption has gained increased popularity in recent years (Secanell et al., 2007; Sun et al., 2005, Rao et al., 2006, 2007; Jain et al., 2008, 2010). Such models, like those developed by Sun et al. (2005), show remarkable agreement with experimental data.

A vital feature of an agglomerate model when applied to low-temperature PEM fuel cells is how the formation of liquid water within the cathode is handled. There are several approaches to modeling liquid water in the cathode catalyst layer. Some models assume that liquid water is not present and, therefore, do not consider it in the modeling equations (Secanell et al., 2007; Sun et al., 2005). Eikerling (2006) presents a set of modeling scenarios that describes, respectively, a dry, optimally wet, and fully flooded catalyst layer. The final case describes a poorly designed catalyst layer in which all void space located between catalyst agglomerates is considered to be flooded with liquid water. Eikerling finds that having the proper pore structure with the appropriate surface wetting properties helps to drive liquid water out of the catalyst layer via primary pores (3–10 nm) leaving secondary pores (10–40 nm) open for reactant gas transport.

Other models have been developed that simultaneously account for the production and transport of liquid water as shown by Das et al. (2010). These models account for water present in the cathode catalyst layer from the oxygen reduction reaction (ORR), electro-osmotic drag through the membrane, and condensation effects due to the relative humidity of inlet gases. However, these models predict significantly different results under similar operating conditions. Pasaogullari and Wang (2004) report liquid saturation on the order of 10–20% in the cathode catalyst layer at a local current density of 1.4 A/cm^2. Under similar operating conditions, Wang and Nguyen (2008) report liquid saturation on the order of 60–80%. Two factors account for this large discrepancy. The former work utilizes Udell's correlation, which was developed for flow through sand, to determine the Leverett function in the capillary flow through porous media relation. Conversely, Wang and Nguyen use an empirical formula for the capillary pressure derived from experiments on a PEM fuel cell catalyst layer. Additionally, Wang and Nguyen correctly account for the differences in capillary properties of the gas diffusion layer (GDL) and cathode catalyst layer (CCL) by introducing a constant capillary pressure boundary condition at the GDL/CCL interface. For these reasons the remainder of this work will utilize the capillary parameters reported as C1 and G1 by Wang and Nguyen (2008).

Numerous mathematical and experimental optimizations of the cathode catalyst layer have been reported over the past few years. Secanell et al. (2007) used an agglomerate model for the catalyst layer microstructure to maximize the current density at three different cell voltages. They found that the optimal microstructure was strongly dependent upon the operating voltage. However, their model neglects the presence of liquid water in the catalyst layer. Kjelstrup et al. (2010) optimized a simplified, pseudo-homogeneous, constant overpotential catalyst layer model with structured macroporosity by maximizing cell voltage at a given current density. They found that, when coupled with a novel gas distribution system, the amount of catalytic material in the resulting catalyst layer could be reduced by a factor 4–8, while increasing energy efficiency 10–20% at high current densities. Friedmann and Nguyen (2010) experimentally optimized the cathode catalyst layer microstructure. They used a two-step catalytic ink preparation method, which allows for the control of the ionomer and gas phases without site blockage by Teflon, which they include in the catalyst ink to facilitate the formation of hydrophobic macropores. They found that a sufficient amount of ionomer is needed to provide a continuous ionic phase, and an optimal amount of Teflon (Teflon:Carbon $=0.5$) with 0.55 mg Pt/cm^2 allowed for a continuous gas phase without agglomerate separation. These conditions led to microstructures with peak power densities of 0.66 W/cm^2. Martin et al. (2010) have developed a catalyst layer preparation technique resulting in an ultra-low platinum-loaded cathode. These catalyst layers have platinum loadings as low as 0.012 mg/cm^2, leading to very high platinum utilization. They also investigated the effects of varied Nafion loadings on cathode performance, showing that 30–50 wt% Nafion loading was optimal.

This work focuses on developing a rational design for the cathode catalyst layer microstructure of a low-temperature PEM fuel cell. The relatively slow intrinsic reaction rate, combined with the presence of liquid water, causes the cathode catalyst layer to be the nexus of a fuel cell's avoidable inefficiencies. Using a one-dimensional agglomerate-liquid saturation model we have performed two optimizations. In one case the microstructure of a PEMFC is optimized to maximize platinum utilization. In the second case the microstructure is optimized to maximize power density.

This work differs from previous mathematical optimizations in that it uses a more rigorous, comprehensive agglomerate model that accounts for the formation and transport of liquid water within the cathode. It will be shown that the inclusion of liquid water in the CCL and cathode GDL has a significant influence on the properties of the optimal microstructures. This work does not include the effects of catalyst deactivation by platinum dissolution; these phenomena will be addressed in later work.

The optimization results can be used to provide rational guidance to the synthesis of a cathode catalyst layer for a PEM fuel cell. The structure of the paper is as follows. First, the geometry of the modeling domain is described along with the design variables, followed by the development of the

mathematical equations. The input parameters are described in Section 3. Next, the simulation procedure is outlined and the objective functions are formally introduced. Finally, the optimization results are presented.

2. Mathematical model of the cathode catalyst layer

2.1. Domain geometry

The cathode catalyst layer is assumed to be composed of many spherical catalyst agglomerates, in which carbon supported platinum is grouped in small spherical pellets bonded by ionomer, Fig. 1. The composition and size of these agglomerates is dictated by the formulation and preparation of the catalyst ink, which is subsequently sprayed onto the gas diffusion layer to form the catalyst layer. In certain instances Teflon is included in the ink to provide continuous hydrophobic pores throughout the catalyst layer to facilitate gas phase transport, but is not specifically modeled in this work. These pores are typically macropores, wider than 50 nm. The catalyst agglomerates have radii that typically range from 50 to 5000 nm (Dobson et al., 2012). The agglomerates within the cathode catalyst layer are treated as a continuum in which the diffusion-reaction equations are solved.

Additionally, the water formed as a result of the ORR at the cathode is accounted for by incorporating a liquid saturation model. Here, a low-temperature PEM fuel cell is considered, therefore, the water that is produced at the cathode is in the liquid phase. This water occupies the void space between agglomerates and is driven out of the catalyst layer primarily by capillary forces. Consequently, the total void volume in the catalyst layer is reduced by the presence of liquid water, which hinders gas phase transport.

The modeling domain includes the gas diffusion layer (GDL), the cathode catalyst layer (CCL) and the polymer electrolyte membrane. Fig. 1 depicts the modeled domain.

2.2. Catalyst layer volume fractions

This section describes the equations that are used to determine the volume fractions of the solid (ε_s^{cl}), ionomer (ε_N^{cl}),and void space (ε_V^{cl}) in the cathode catalyst layer.

Determination of the volume fractions in the CCL begins with allowing the void fraction to directly be a design variable:

$$\varepsilon_V^{cl} = \text{Input parameter}$$

This void fraction is to be interpreted as the volume in the catalyst layer is available for the formation of macropores between catalyst agglomerates. From this we can calculate the solid phase volume fraction, which accounts for the carbon and platinum content of the catalyst layer. Platinum loading m_{pt}, and platinum to carbon ratio, Pt|C, along with catalyst layer thickness, t_{cl} are needed to calculate ε_s^{cl}. To do so it is assumed that all spaces in the catalyst layer that is not occupied by voids are occupied by agglomerates (including their ionomer film) and that the agglomerates are composed of platinum, carbon and ionomer only, see Fig. 1. With this information the solid phase volume fraction is given by

$$\varepsilon_s^{cl} = \left(\frac{1}{\rho_{Pt}} + \frac{1-\text{Pt|C}}{\text{Pt|C}\rho_{Pt}}\right)\frac{m_{Pt}}{t_{cl}} \tag{1}$$

where Pt|C is termed the platinum-to-carbon ration and is defined as the mass of platinum per unit mass of platinum plus carbon in the catalyst layer. Additionally, ρ_{Pt} and ρ_c are the density of platinum and carbon, respectively.

It is now possible to calculate the catalyst layer ionomer (Nafion) fraction. Ionomer is present both inside the agglomerate and in the surrounding agglomerate film. This fraction is calculated from the following expression:

$$\varepsilon_N^{cl} = 1-\varepsilon_s^{cl}-\varepsilon_V^{cl} \tag{2}$$

Finally, the volume fraction of ionomer present in the agglomerate (not including the film) is needed for the computation of $D_{O_2}^{N,eff}$, which is further discussed in Section 3.1. This value is determined by geometric considerations, based on the overall catalyst layer ionomer fraction, void fraction, and solids fraction, as follows:

$$\varepsilon_{N,agg}^{cl} = \left[1-\frac{\varepsilon_s^{cl}(r_{agg}+\delta_{agg})^3}{(1-\varepsilon_N^{cl})(r_{agg})^3}\right] \tag{3}$$

where r_{agg} is the radius of the catalyst agglomerates and δ_{agg} is the ionomer film thickness surrounding each agglomerate.

This set of equations differs from those presented by Secanell et al. (2007) in that $\varepsilon_{N,agg}^{cl}$ is no longer an input parameter, instead being replaced by ε_V^{cl} as an input. Its value is now determined as a consequence of the catalyst layer void fraction, platinum loading, platinum-to-carbon ratio, and catalyst layer thickness. This was done such that the catalyst layer void fraction does not depend on agglomerate ionomer fraction. For a given agglomerate radius, the composition of that agglomerate should not alter the void fraction of the catalyst layer.

2.3. Primary design variables

This section gives a brief description of the design variables used in the optimization of a PEM fuel cell catalyst layer. Independent manipulation of any of these variables affects the performance of the cathode catalyst layer by influencing several different phenomena, both directly (primary effect) and indirectly (secondary effects), as a result of the coupled nature of the design equations. For instance, an increase in platinum loading results in a primary effect of higher surface area available for reaction leading to a higher intrinsic reaction rate. However, the same change influences several other parameters as well, including the solids, ionomer, and void volume fractions.

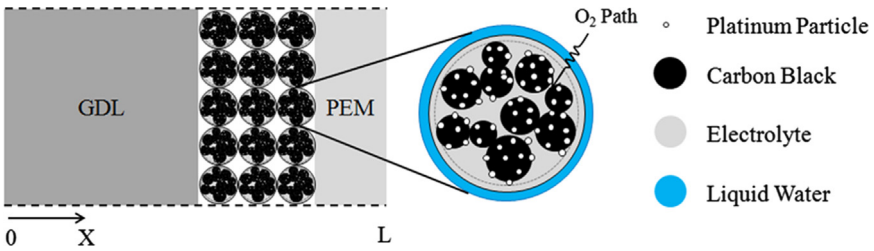

Fig. 1. Modeling domain of the PEM fuel cell. Model includes cathode gas diffusion layer (GDL), cathode catalyst layer (CCL) and polymer electrolyte membrane (PEM). The catalyst layer is composed of spherical agglomerates each surrounded by a liquid water film. The thickness of the catalyst layer is exaggerated. $x=L$ corresponds to the interface between the membrane and the anode catalyst layer. $x=0$ corresponds to the interface between the cathode gas channel and the cathode GDL.

2.3.1. Platinum loading (m_{Pt})

Platinum loading is a critical parameter that dictates the maximum intrinsic catalytic activity of the catalyst layer. Typical values of platinum loading for the cathode catalyst layer of a PEM fuel cell range from 0.2 to 0.8 mg/cm^2 (Litster and McLean, 2004). High platinum loadings lead to a fast intrinsic reaction rate by providing additional catalytic surface area for the oxygen reduction reaction. However, this increased reaction rate can lead to severe diffusion limitations, resulting in a low effectiveness factor. Low platinum loadings reduce diffusion limitations by slowing the reaction rate, but too low a loading limits the overall reaction rate leading to insufficient power densities.

2.3.2. Platinum-to-carbon ratio (Pt|C)

Platinum-to-carbon ratio determines how much carbon black exists in the catalyst layer for a given platinum loading. This ratio plays a key role in how well the platinum is dispersed over the carbon black surface as reported by Marr and Li (1999), as well as in the solids and ionomer volume fractions. In this study Pt|C was allowed to vary between 0.10 and 0.90.

2.3.3. Catalyst layer void fraction (ε_V^{cl})

The catalyst layer void fraction represents the volume of the catalyst layer available for the formation of macropores between the catalyst agglomerates. These macropores permit reactant gases to diffuse into the catalyst layer, as well as product water to be transported out of the catalyst layer. Secanell et al. (2007) report that for the pores to remain connected as a percolating network the total void volume fraction must remain above 0.25.

2.3.4. Agglomerate radius (r_{agg})

While not explicitly optimized in this work, the radius of the catalyst agglomerates is pivotal to the overall performance of the cell, as it accounts for one of the two main transport limitations in the system, namely intra-agglomerate diffusion limitations. Broka and Ekdunge (1997) report agglomerate radii ranging between 0.5 and 2.5 μm based on the scanning electron micrographs of a PEM fuel cell catalyst layer. Malek et al. (2007) simulated a catalyst layer of a PEM fuel cell and found that the agglomerates can be as small as 50 nm. When included in the optimization the optimal agglomerate radius yields only the trivial solution in which the smallest allowed agglomerate performs best. Agglomerate radii less than 25 nm are not considered in this work, as the approximation of an agglomerate as a continuum with effective properties becomes invalid when the aspect ratio of a system is below 5:1 (Sahimi et al., 1990). The effect of agglomerate radius is further discussed in Section 5.3.

For this study the thickness of the catalyst layer (t_{cl}) was assumed to be a function of the platinum loading. This is consistent with most fabrication methods, which involve spraying on multiple layers of catalyst ink to achieve a desired loading. Here, we assume an incremental catalyst layer thickness of 1 μm per 0.01 mg/cm^2 of platinum loading.

2.4. Model assumptions

The following assumptions are made in the modeling of the phenomena occurring in the cathode catalyst layer:

- Fuel cell is operating at steady state
- Gases are ideal
- System is isothermal at 353 K and isobaric at 1.5 bar
- Inlet air is saturated at 100% relative humidity
- Fully saturated Nafion phase in the CCL and membrane
- Uniform catalyst pellet size and uniform Nafion film thickness on the pellets

Table 1
Parameters for the capillary pressure correlation in the gas diffusion and catalyst layer (Wang and Nguyen, 2008).

Capillary function	$a1$	$a2$	b (Pa)	c	d (Pa)
GDL	−17.3	−25.1	−32.3	0.35	−4.06
CCL	−23.5	−17.4	477	0.46	−3.58

- Membrane is impermeable to gas species
- Oxygen transport in the catalyst layer is modeled by Fick's law
- Electronic conduction of the GDL and CCL is high enough to neglect their electronic resistance
- Overpotential of the hydrogen oxidation reaction at the anode is negligible

These assumptions are consistent with those described in many prior catalyst layer modeling studies (Wang and Nguyen, 2008; Secanell et al. 2007; Sun et al. 2005).

2.5. Agglomerate – saturation model equations

This work utilizes a modified one-dimensional liquid saturation model initially developed by Lin et al. (2004) and Wang and Nguyen (2008). The model describes the steady-state, two-phase mass transport and reaction in the cathode of a PEMFC. The modeling domain consists of the gas diffusion layer, cathode catalyst layer, and polymer electrolyte membrane. Reactant oxygen diffuses from the gas channels through the gas diffusion layer and into the catalyst layer where it reacts to form liquid water. In addition, electro-osmotic drag and condensation/evaporation of liquid water within the cathode catalyst layer are described. A summary of the governing equations of this model is provided below. For more details, the reader is referred to Wang and Nguyen (2008). There are four variables in this model:

1. $C_{O_2}^g$, concentration of oxygen gas (mol/m^3)
2. C_v^g, concentration of water vapor (mol/m^3)
3. ϕ_m, ionic phase potential (V)
4. s_{cl}, liquid water saturation level in the catalyst layer

As a simplification to the model of Wang and Nguyen (2008), we assume that the liquid water saturation level in the gas diffusion layer is constant and that all Nafion are fully saturated with water. Furthermore, the reaction rate term is modified to account for the spherical geometry of the catalyst agglomerates.

The fluxes of gaseous species ($i = O_2$ or water vapor) in the gas diffusion and catalyst layers are expressed by

$$N_i^g = -D_i^{g,eff}\nabla C_i^g \tag{4}$$

where $D_i^{g,eff}$ is the effective diffusivity of gas species in the void space of the gas diffusion or cathode catalyst layer. The flux of liquid water due to capillary flow is given by

$$N_w = C_w\nu = \frac{\rho_w}{M_w}\left(\frac{-K_w(s_j)}{\mu_w}\nabla P_{l,j}\right) \tag{5}$$

where the subscript "j" refers to either the gas diffusion layer (GDL) or the cathode catalyst layer (CCL). P_l is the capillary pressure in either the gas diffusion or catalyst layer and is given by the following experimentally determined correlation for capillary pressure (Wang and Nguyen, 2008):

$$P_c(s) = P_g - P_l = d[e^{-a_1(s-c)} - e^{a_2(s-c)}] + b \tag{6}$$

where s is the saturation level in the domain of interest and a_1, a_2, b, c, d are fitting parameters within that domain. In Eq. (3) P_g is the gas phase pressure, which is assumed to be constant. Table 1 summarizes the parameters used in Eq. (6).

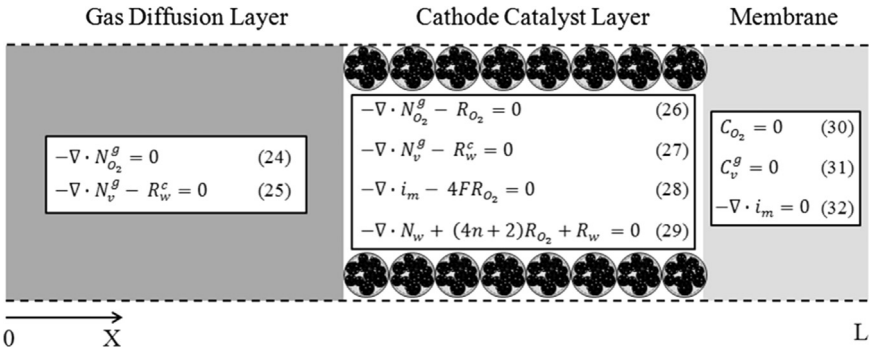

Fig. 2. Summary of modeling equations in each domain of the low-temperature PEMFC model. Domains are not drawn to scale.

The effective diffusion coefficients, $D_i^{g,eff}$, are calculated using the following effective medium approximation:

$$D_i^{g,eff} = D_j^g[\varepsilon_j^v(1-s_j)]^{1.5} \tag{7}$$

This correction also accounts for the presence of liquid water in the catalyst and gas diffusion layer, which further inhibits transport.

Additionally, the permeability of both the gas diffusion and cathode catalyst layers depends on the liquid water saturation as

$$K_w(s) = K_{w,0}s^{4.5} \tag{8}$$

By substituting Eqs. (6) and (8) into Eq. (5) the expression for the liquid water flux can be re-written as

$$N_w = \frac{-\rho_w K_{w,0}}{M_w\mu_w}s^{4.5}\frac{dP_c}{dx} = \frac{-\rho_w K_{w,0}}{M_w\mu_w}\frac{dP_c}{ds}s^{4.5}\frac{ds}{dx} \tag{9}$$

Wang and Nguyen (2008) group the parameters in the prefactor to the saturation gradient into a term that they call the capillary diffusion coefficient, D_c

$$D_c = \frac{-K_{w,0}}{\mu_w}\frac{dP_c}{ds}s^{4.5} \tag{10}$$

With this, Eq. (5) can be re-written as

$$N_w = -D_c\frac{\rho_w}{M_w}\frac{ds}{dx} \tag{11}$$

Furthermore, the rate of water phase change (mol/m^3 s) in the GDL and CCL is described by Wang and Nguyen (2008) as

$$R_w^c = k_c\frac{\varepsilon_i^V(1-s)y_v}{RT}(y_vP-P_v^{sat})q + k_v\frac{\varepsilon_i^V s\rho_w}{M_w}(y_vP-P_v^{sat})(1-q) \tag{12}$$

where y_V is the mol fraction of liquid water, ρ_w is the density of liquid water, M_w is the molecular weight of water and q is a switching function that activates either the condensation or the evaporation term, depending on the local cell condition:

$$q = \frac{1+[|(y_vP-P_v^{sat})|/(y_vP-P_v^{sat})]}{2} \tag{13}$$

The reaction rate for the oxygen reduction reaction (mol/cm^3 s) in the spherical agglomerates within the cathode catalyst layer is given by

$$R_{O_2} = \left[\frac{RT/H_{O_2}^w}{(\delta_w(\delta_N+r_{agg})/(\delta_w+\delta_N+r_{agg})a_rD_{O_2}^N) + (\delta_w r_{agg}/(\delta_N+r_{agg})a_rD_{O_2}^N + (1/\xi k_t))}\right]C_{O_2} \tag{14}$$

where $H_{O_2}^w$ is Henry's law constant for oxygen and water (atm m^3/mol), δ_N is the ionomer film thickness surrounding an agglomerate (m), a_r is the effective agglomerate surface area (m^2/m^3), $D_{O_2}^N$ is the diffusivity of oxygen within an agglomerate (m^2/s), δ_w is the water film thickness surrounding an agglomerate (m), ξ is the catalyst layer effectiveness factor, and k_t is the reaction rate constant (s^{-1}). A further description of these terms is to follow. Eq. (14) is similar to that derived by Wang and Nguyen (2008), however it has been altered to reflect spherical agglomerate geometry. The first term in the denominator accounts for the diffusion of oxygen through the water film surrounding the agglomerate. The second term in the denominator accounts for diffusion through the ionomer film, and the final term accounts for diffusion and reaction inside the agglomerate. The reaction rate constant is given by

$$k_t = (1-\varepsilon_V^{cl})\frac{a_{Pt}^{agg}i_0^{ref}}{4FC_{O_2}^{ref}}\exp\left[\frac{\alpha_cF}{RT}(V_A-\Phi_m-U_{ref})\right] \tag{15}$$

Here, V_A is the applied fuel cell potential and a_{Pt}^{agg} is the active catalyst surface area per unit volume of agglomerates, defined as

$$a_{Pt}^{agg} = \frac{a_{Pt}m_{Pt}}{t_{cl}(1-\varepsilon_V^{cl})} \tag{16}$$

with a_{Pt} the surface area per unit mass of Pt (cm^2/g Pt). This study uses an empirical correlation for an E-TEK catalyst layer developed by Secanell et al. (2007) to estimate the value

$$a_{Pt} = 2.2779\times10^6(\text{Pt|C})^3 - 1.5857\times10^6(\text{Pt|C})^2 - 2.0153\times10^6(\text{Pt|C}) + 1.595\times10^6 \tag{17}$$

where Pt|C is the platinum to carbon ratio in an individual agglomerate.

In Eq. (14) the effectiveness factor ξ is expressed by

$$\xi = \frac{1}{\varphi}\left(\frac{3\varphi\coth(3\varphi)-1}{3\varphi}\right) \tag{18}$$

where the Thiele modulus is given by

$$\varphi = \frac{r_{agg}}{3}\sqrt{\frac{k_t/(1-\varepsilon_V^{cl})}{D_{O_2}^{N,eff}}} \tag{19}$$

The water film thickness is related to the liquid saturation level in the catalyst layer as (Wang and Nguyen, 2008)

$$\delta_w = \frac{\varepsilon_V^{cl}s_{cl}}{a_r} \tag{20}$$

where a_r represents the outer surface area of the spherical agglomerates per unit catalyst agglomerate volume and is calculated by

$$a_r = \frac{3}{r_{agg}}(1-\varepsilon_V^{cl}) \tag{21}$$

The water flux in the membrane is a function of both concentration gradient and electro-osmotic drag terms:

$$N_w^N = \frac{i_d n}{F} - D_w^N\nabla C_w^N \tag{22}$$

Here, n is the electro-osmotic drag coefficient. Furthermore, by assuming that the membrane is fully saturated, the concentration gradient term in Eq. (22) can be neglected.

Table 2
Parameters used in PEMFC cathode model.

Geometry	***Value***	***Units***	***Source***	***Parameter***	***Value***	***Units***	***Source***
δ_{GDL}	250	μm	Secanell et al. (2007)	r_{agg}	150	nm	Wang and Nguyen (2008)
δ_{mem}	50	μm	Secanell et al. (2007)	δ_{agg}	12	nm	
Operating conditions							
P	1.5	atm	Secanell et al. (2007)	x_{O2}	0.11	–	Secanell et al. (2007)
T	353	K	Parthasarathy et al. (1992)	x_{N2}	0.42	–	Secanell et al. (2007)
U_{ref}	1.0	V	Secanell et al. (2007)	x_W	0.47	–	Secanell et al. (2007)
Evaporation rate constant (k_v)	100	1/(atm s)	Secanell et al. (2007)	Condensation rate constant (k_c)	100	1/s	Secanell et al. (2007)
Physical properties							
$C_{O2,ref}$	0.85	mol/cm^3	Parthasarathy et al. (1992)	$\varepsilon_{v,GDL}$	0.75	–	Parthasarathy et al. (1992)
$i_{0,273}$	1.0×10^6	A/cm^2	Secanell et al. (2007)	ρ_c	21.5	g/cm^3	Parthasarathy et al. (1992)
i_0	$i_{0,273}2^{(T-273)/10}$	A/cm^2	Parthasarathy et al. (1992)	ρ_{Pt}	2.0	g/cm^3	Parthasarathy et al. (1992)
α	1.0	–	Parthasarathy et al. (1992)	$H_{02,N}$	3.56×10^5	atm cm^3/mol	Sander (1999)
λ	$C_{w,N}/C_f$	–	Parthasarathy et al. (1992)	$H_{02,W}$	7.80×10^5	atm cm^3/mol	Sander (1999)
n	(2.5/22)λ	–	Parthasarathy et al. (1992)	P_{sat}	0.467	atm	Secanell et al. (2007)
μ_w	0.35	cP	Parthasarathy et al. (1992)	$C_{w,N}$	4.2×10^{-3}	mol/cm^3	Secanell et al. (2007)
C_f	1.2×10^{-3}	mol/cm^3	Parthasarathy et al. (1992)				
Bulk transport properties							
$D_{O2,g}$	2.89×10^{-1}	cm^2/s	Secanell et al. (2007)	$D_{V,g}$	3.73×10^{-1}	cm^2/s	Secanell et al. (2007)
$D_{O2,N}$	8.45×10^{-5}	cm^2/s	Secanell et al. (2007)	$K_{w,0-GDL}$	2.0×10^{-11}	cm^2	Secanell et al. (2007)
$D_{O2,w}$	4.73×10^{-5}	cm^2/s	Secanell et al. (2007)	$K_{w,0-CL}$	5.0×10^{-13}	cm^2	Secanell et al. (2007)
k_N	0.089	S/cm	Secanell et al. (2007)				

The ionic flux is expressed by

$$i_m = -k_N \nabla \Phi_m \tag{23}$$

Fig. 2 provides a summary of the governing equations for each domain.

2.6. Boundary conditions

As shown in Fig. 1 the modeling domain extends from $x=0$ at the gas channel|GDL interface to $x=L$ at the membrane|anode catalyst layer interface. The model of Wang and Nguyen (2008) utilizes a constant capillary pressure boundary condition at the GDL|CCL interface. The boundary conditions for each of the dependent variables are described below.

The boundary conditions at the gas channel|GDL interface are

$$C^g_{O_2} = C^{air}_{O_2} \tag{33}$$

$$C^g_v = C^{g,air}_v \tag{34}$$

The boundary conditions at the GDL|CCL layer interface are

$$N^g_{O_2}|_{GDL} = N^g_{O_2}|_{CCL} \tag{35}$$

$$N^g_v|_{GDL} = N^g_v|_{CCL} \tag{36}$$

$$i_m|_{CCL} = 0 \tag{37}$$

$$P_c|_{GDL} = P_c|_{CCL} \tag{38}$$

The boundary conditions at the CCL|membrane interface are

$$N^g_{O_2}|_{CCL} = 0 \tag{39}$$

$$N^g_v|_{CCL} = 0 \tag{40}$$

$$i_m|_{CCL} = i_m|_{MEM} \tag{41}$$

$$N_w|_{CCL} = N^N_w|_{MEM} \tag{42}$$

The boundary conditions at the embrane|anode catalyst layer interface are

$$C^g_{O_2} = 0 \tag{43}$$

$$C^g_v = 0 \tag{44}$$

$$\Phi_m = 0 \tag{45}$$

3. Model input parameters

Table 2 summarizes the various parameters used in this model including bulk transport parameters.

3.1. Transport parameters

Many methods have been explored to determine effective transport parameters in PEM fuel cells, including effective medium theory (Secanell et al., 2007), pore-network modeling (Evans et al., 1980) and Monte-Carlo simulations. In this work Bruggeman's effective medium approximation is used to describe the transport of oxygen in the porous cathode, via Eq. (7). This assumes the following relationship between porosity and tortuosity:

$$\tau_i = \sqrt{\frac{1}{\varepsilon_i}} \tag{46}$$

This same correlation is extended to describe the effective conductivity in the catalyst layer and the effective diffusivity of oxygen within an agglomerate:

$$k^{eff}_N = k_N \frac{\varepsilon^{cl}_V}{\tau_{cl}} \tag{47}$$

$$D^{N,eff}_{O_2} = D^N_{O_2} \frac{\varepsilon^{agg}_N}{\tau_{agg}} \tag{48}$$

It is important to note, however, that the Bruggeman approximation is no longer reliable when volume fractions become very small. In a fuel

cell catalyst layer it is vital that all three phases exist above their percolation threshold to ensure reasonable transport. Experimental studies have shown that the percolation threshold of a typical catalyst layer is 0.12, similar to that of the packing structure of an FCC lattice as demonstrated by Secanell et al. (2007). As a consequence, the optimal design must be further constrained, such that the total solids fraction is above 0.12. Similarly, the total void fraction must remain above 0.25 to ensure a percolating network under saturated conditions.

4. Simulation procedure

The primary goal of this work is to manipulate the parameters that make up the microstructure, so as to maximize the platinum utilization (kilowatts of electricity per gram of platinum catalyst). The Department of Energy has stated goals for platinum utilization of 3.0 kW/g by 2010 and 8.0 kW/g by 2015.

4.1. Microstructure optimization – platinum utilization (kW/g Pt)

The corresponding objective function captures the desire for high power density at low platinum loading, and is defined as follows:

$$\min_{(m_{pt},Pt|C,\varepsilon_V^{cl})} \left[\frac{4FV_A\int_{L-t_{cl}}^{L} R_{O_2}\,dx}{m_{Pt}}\right] \tag{49}$$

S.t.

$$0.12 < \varepsilon_s^{cl} < 1, \quad 0.12 < \varepsilon_N^{cl} < 1$$
$$0.25 < \varepsilon_V^{cl} < 1, \quad P_d > 0.20\ \mathrm{W/cm^2}$$

These constraints ensure that each phase (solid, ionomer, gas) remains above its percolation threshold. The constraint on minimum power density is present to ensure that the resulting microstructure can provide substantial power while maintaining the overall cell and stack size at reasonable dimensions.

4.2. Simulation procedure

The modeling domain described in Fig. 1 was modeled using the finite element solver COMSOL 3.5a. The multivariable optimizations were performed using the *fmincon* optimizer in Matlab 2008a in conjunction with COMSOL 3.5a. The interior-point algorithm with the default tolerances was used for the constrained optimizations. The aforementioned constraints were implemented as a series of nonlinear constraints. Each optimization took approximately 120 s on a DELL Precision T3500 workstation operating LINUX with 4GB of RAM and a 2.66 GHz Intel quad-core processor. Table 3 summarizes the upper and lower bounds on the design variables.

Table 3
Optimization bounds for design parameters.

Design variable	Lower bound	Upper BOUND
m_{Pt} (mg/cm^2)	0.01	1.0
Pt|C	0.10	0.90
ε_V^{cl}	0.25	1.0

5. Results and discussion

5.1. Optimization of platinum utilization

Table 4 summarizes the platinum utilization optimization results when m_{Pt}, Pt|C, and ε_V^{cl} are all allowed to vary. The optimized catalyst layer utilizes an ultra-low platinum loading with a low platinum-to-carbon ratio. This results in a platinum utilization that is nearly 30 times higher than the most commercially available catalyst layers (Litster and McLean, 2004). This comes from a high surface area of platinum per unit platinum mass associated with a low Pt|C. To compensate for ultra-low platinum loading the catalyst layer must become very thin to ensure a percolating solids fraction. Here, the optimum catalyst layer thickness is 1.0 μm for an applied cell voltage of 0.40 V. Included in Table 4 are also the results from optimization of the same model without liquid water. Furthermore, very recent reports suggest that the oxygen transport resistance increases linearly with decreased platinum loading (Greszler et al., 2012; Sakai et al., 2009; Ono et al., 2010). Causes for this remain unclear; however, we investigated the effects of such increased resistance on our results. The optimum parameters are not significantly altered – ultra-low platinum loadings are still optimal – but the maximum power density is decreased from 0.36 W/cm^2 to 0.24 W/cm^2. Fig. 3 shows the polarization curves for the various microstructures studied. The microstructures that incorporate the presence of liquid water show diminished performance, primarily as a result of oxygen dissolution in water as opposed to Nafion.

Fig. 4a and b shows that the primary difference between a conventional design and the design with optimized platinum utilization comes from reducing the diffusion limitations inside agglomerates. In a conventional design the platinum catalyst present at the center of an agglomerate is exposed to extremely low oxygen concentrations – thus underutilizing this catalyst. When an ultra-low amount of platinum is used, an appreciable oxygen concentration remains present along the entire radius of the agglomerate. Fig. 5 shows the enhanced platinum utilization of the optimal design compared to conventional catalyst layer microstructures with respect to platinum utilization over a range of operating voltages. Fig. 6 shows that the ultra-low platinum loading microstructure leads to very similar power densities to the base microstructure over that same range of operating voltages. The optimum operating point occurs at $V_A \sim$ 0.40 V. At this point the optimized microstructure yields a platinum utilization that is over 30 times higher than conventional designs, while maintaining a power density that is nearly 80% (53% with low m_{Pt} transport resistance correction in model) that of the base microstructure.

This dramatic increase in platinum utilization, while maintaining appreciable power density ($>$0.24 W/cm^2 and 0.36 W/cm^2 with and without the low platinum loading transport resistance correction respectively), could have a transformative impact on reducing the cost of PEM fuel cell electrodes.

It must be noted, however, that the use of such low catalyst loadings might lead to catalyst layer durability problems. As the limited amount of platinum begins to deactivate, dissolve and aggregate over time, the remaining active catalyst surface area may quickly become insufficient to sustain the desired operating conditions. The presented optimization studies are therefore being extended to account for the effects of platinum deactivation, dissolution and aggregation. Additionally, work is currently underway to provide experimental validation to the model-predicted performances for ultra-low platinum loadings, as well as determining decay rates at different catalyst loadings.

5.2. Effect of the optimized structure on liquid saturation

Management of liquid water in the cathode of a low-temperature PEM fuel cell is a vital component of a robust and high performance design. Excessive liquid water in the cathode leads to poor mass transport of reactant gases, see Eq. (7), thus reducing cell performance. Fig. 7 shows the liquid water saturation (m^3 water/m^3 void space) profiles in the catalyst layer for both the base and the optimized microstructures.

Table 4
Results of microstructure optimization to maximize platinum utilization in the cathode catalyst layer. $V_A = 0.40$ V.

Cathode Model	m_{Pt} (mg/cm^2)	t_{cl} (μm)	Pt|C	ε_s^{cl}	ε_v^{cl}	ε_N^{cl}	$\varepsilon_{N,agg}$	i_d (A/cm^2)	P_d (W/cm^2)	*Pt Utilization* (kW/g Pt)
Base design	0.40	40	0.28	0.13	0.50	0.37	0.66	1.16	0.46	1.20
Optimized microstructure	0.01	1.0	0.27	0.14	0.25	0.61	0.77	0.91	0.36	36.3
Opt. w/no liquid water	0.01	1.0	0.23	0.17	0.28	0.55	0.71	1.17	0.47	46.7
Opt. w/low m_{Pt} correction	0.01	1.0	0.26	0.15	0.27	0.58	0.75	0.54	0.24	20.8

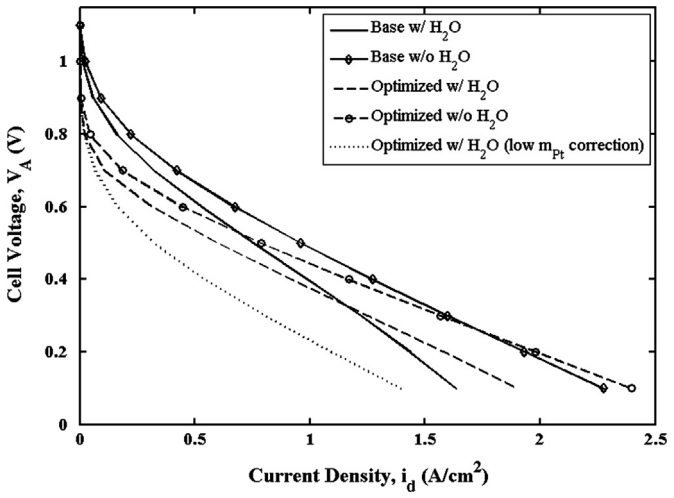

Fig. 3. Polarization curves for multiple cathode catalyst layer microstructures considered in this work. Platinum loading of base and optimized microstructures is 0.40 mg/cm^2 and 0.01 mg/cm^2, respectively.

It is seen that the thin catalyst layer (~1 μm) of the optimized microstructure displays a lower average water saturation level compared to the much thicker (>40 μm) base microstructure. Close inspection reveals that the two curves are nearly identical for the first 1 μm, measured from the GDL|CL interface, and that significantly more water builds up in the additional thickness of the base microstructure.

5.3. Effect of agglomerate radius

The agglomerate radius plays a significant role in the performance of the cathode catalyst layer. Wang and Nguyen (2008) use a unique agglomerate radius of 100 nm in their liquid saturation model. Sun et al. (2005) also assume a unique agglomerate radius in their catalyst layer model; however, they use a value of 1000 nm. Dobson et al. (2012) have reported values between 50 and 5000 nm throughout various studies.

As previously mentioned, the agglomerate radius is not included as an explicit design variable in this work. However, several optimizations were run for various agglomerate radii to show the dramatic performance improvements that could be made by utilizing smaller agglomerates. Smaller radii reduce (or eliminate) diffusion limitations within the agglomerates themselves, thus increasing the overall rate of reaction, and yielding effectiveness factors approaching 1 throughout the catalyst layer, see Figs. 8 and 9, where the simulations are run at $V_A = 0.40$ V. As a result of the increased reaction rate within an agglomerate, the diffusion limitations along the length of the catalyst layer become more prominent. Additionally, the increased reaction rate causes a larger flux of protons through the membrane from the anode. This rise in ionic flux results in more severe Ohmic losses within the membrane, thus reducing the cathodic rate coefficient. This can be seen in Fig. 10. Reducing the size of the agglomerates from 1 μm to 25 nm can further increase the platinum utilization by a factor of four. Fig. 11 shows optimization results for various agglomerate

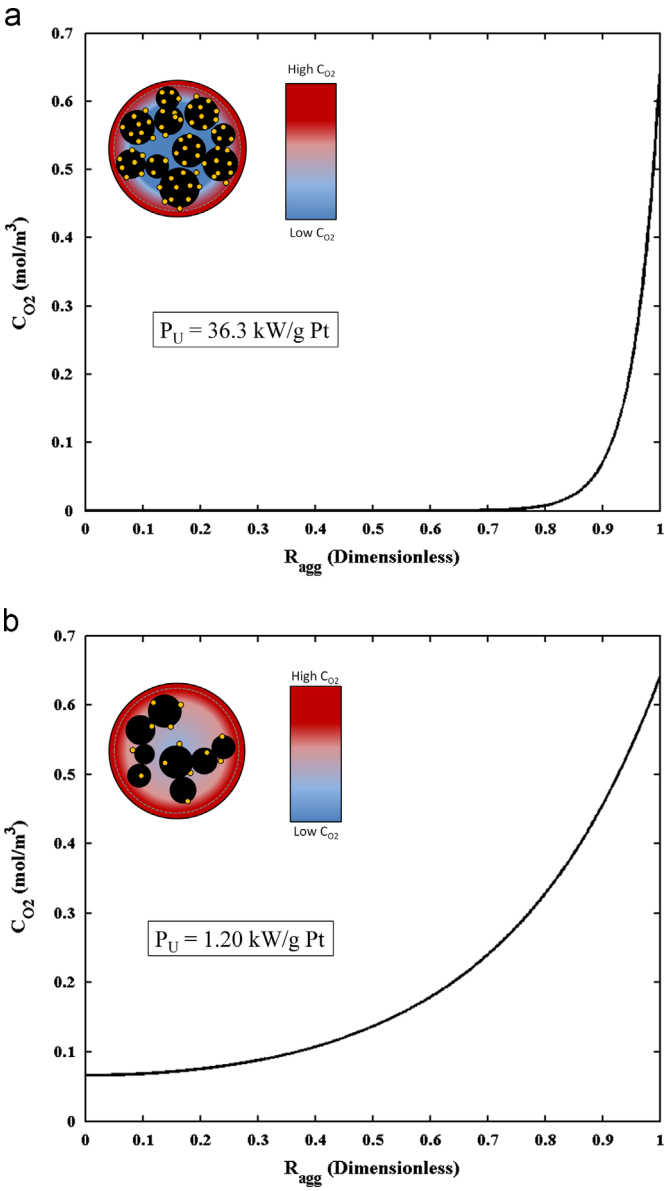

Fig. 4. (a) Dissolved oxygen concentration in a single agglomerate in a catalyst layer with $m_{Pt} = 0.40$ mg/cm^2. Cell operating at $V_A = 0.40$ V. (b) Dissolved oxygen concentration in a single agglomerate in a catalyst layer with an ultra-low platinum loading, $m_{Pt} = 0.010$ mg/cm^2. Cell operating at $V_A = 0.40$ V.

radii. The platinum utilization increases linearly with decreasing agglomerate radius until the system begins to display kinetic limitations at $r_{agg} < 50$ nm. For much smaller agglomerates, there are no longer significant diffusion limitations within them and the rate of reaction is limited by the intrinsic kinetics of the oxygen reduction reaction on the platinum catalyst surface.

By decreasing the agglomerate size and utilizing ultra-low platinum loadings, the platinum utilization can be improved by a

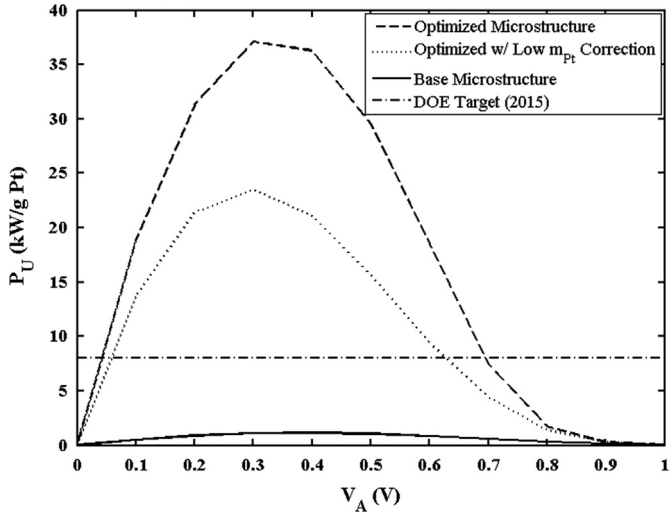

Fig. 5. Comparison of platinum utilization over a range of operating voltages for baseline and optimized microstructures. Baseline parameters: $m_{Pt} = 0.40$ mg/cm^2, PtIC $= 0.28$, $t_{cl} = 40$ μm, $\varepsilon_V^{cl} = 0.50$. Optimum parameters: $m_{Pt} = 0.01$ mg/cm^2, PtIC $= 0.27$, $t_{cl} = 1.0$ μm, $\varepsilon_V^{cl} = 0.25$.

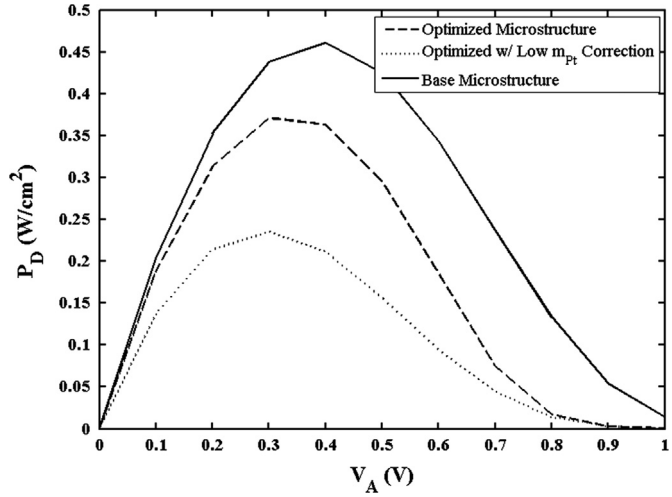

Fig. 6. Comparison of power density over a range of operating voltages for baseline and optimized microstructures. Baseline parameters: $m_{Pt} = 0.40$ mg/cm^2, PtIC $= 0.28$, $t_{cl} = 40$ μm, $\varepsilon_V^{cl} = 0.50$. Optimum parameters: $m_{Pt} = 0.01$ mg/cm^2, PtIC $= 0.27$, $t_{cl} = 1.0$ μm, $\varepsilon_V^{cl} = 0.25$.

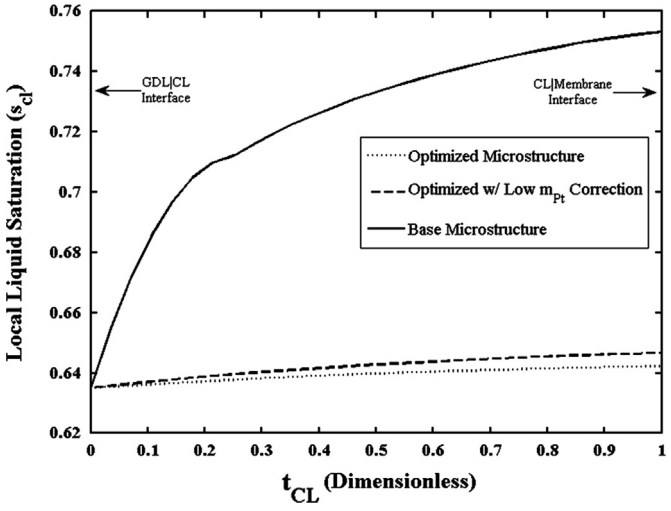

Fig. 7. Comparison of local liquid water saturation levels in base microstructure ($t_{cl} = 40$ μm) versus ultra-low platinum loading microstructure ($t_{cl} = 1.0$ μm). Cell operating at $V_A = 0.40$ V; $t_{cl} = 0$ corresponds to GDL|CL interface.

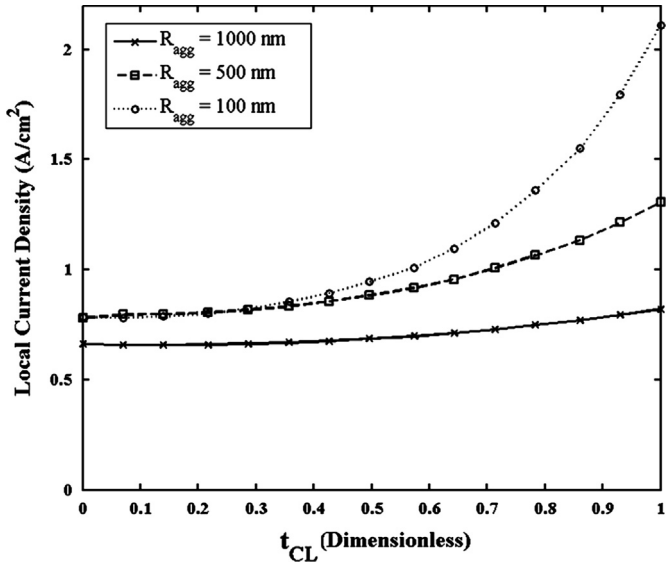

Fig. 8. Local current density profiles for varying agglomerate radius. Here, t_{cl}, m_{Pt}, PtIC and ε_V^{cl} are held constant at 15 μm, 0.40 mg/cm^2, 0.28, and 0.25, respectively. $V_A = 0.4$ V; $t_{cl} = 0$ corresponds to GDL|CL interface.

factor of 30 over traditional catalyst layer compositions while still maintaining power densities above 0.35 W/cm^2.

The size of the catalyst agglomerates also influences the liquid saturation level in the catalyst layer. Fig. 12 shows the effect of agglomerate radius on the local saturation profiles with the optimized microstructured catalyst layers. Smaller radii lead to higher effectiveness factors that increase the overall reaction rate throughout the catalyst layer, thus increasing the amount of water present along the length of the catalyst region. It should be noted that the choice of agglomerate radius influences the pore size distribution in the catalyst layer, which alters the capillary properties. However, for this work a simplifying assumption was made of constant capillary properties at each value of r_{agg} studied.

6. Conclusion

This paper presented results on the optimization of the cathode catalyst layer of a low-temperature PEM fuel cell with respect to platinum utilization. Careful control of catalyst layer microstructure can significantly enhance cell performance. The optimum microstructure exhibits a balance between the numerous phenomena that are occurring within the catalyst layer. Efficient gas transport is achieved by creating a catalyst layer with a void fraction that remains above the percolation threshold when liquid water saturation is accounted for. Electronic transport is ensured to cause minimal losses by maintaining the solids fraction above 0.15 (Secanell, 2007). Good ionic transport is maintained by having an ionomer fraction in the catalyst layer of roughly 0.60. While this Nafion volume fraction is high compared to other values reported in literature, the ultra-low platinum loading found in this work allows for this higher ionomer fraction due to the reduced intrinsic reaction rate. This lower reaction rate diminishes the effect of diffusion limitations that would otherwise be brought on by high Nafion loadings.

A careful balance between these phenomena is paramount to the efficient operation of the cathode catalyst layer in a PEM fuel cell. It was found that an ultra-low platinum loading in a thin catalyst layer is beneficial to obtain high platinum utilization.

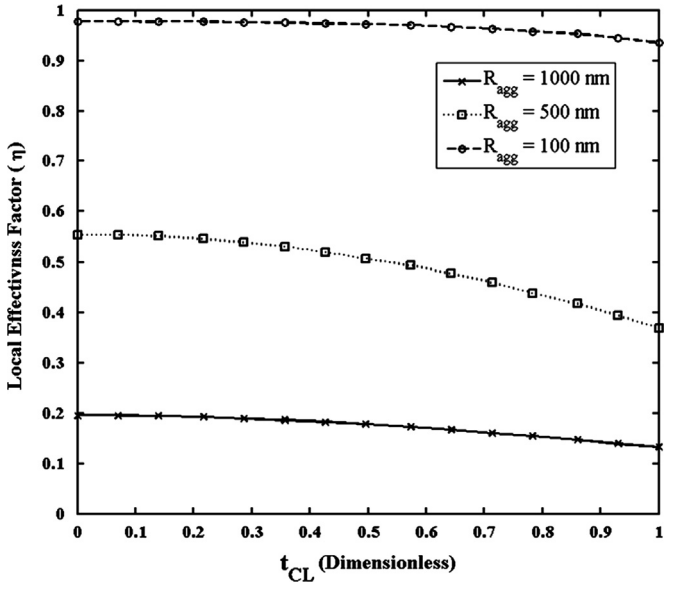

Fig. 9. Local effectiveness factor profiles for varying agglomerate radius. Here, t_{cl}, m_{Pt}, Pt|C and ε_V^{cl} are held constant at 15 μm, 0.40 mg/cm^2, 0.28, and 0.25, respectively. $V_A = 0.4$ V, $t_{cl} = 0$ corresponds to GDL|CL interface.

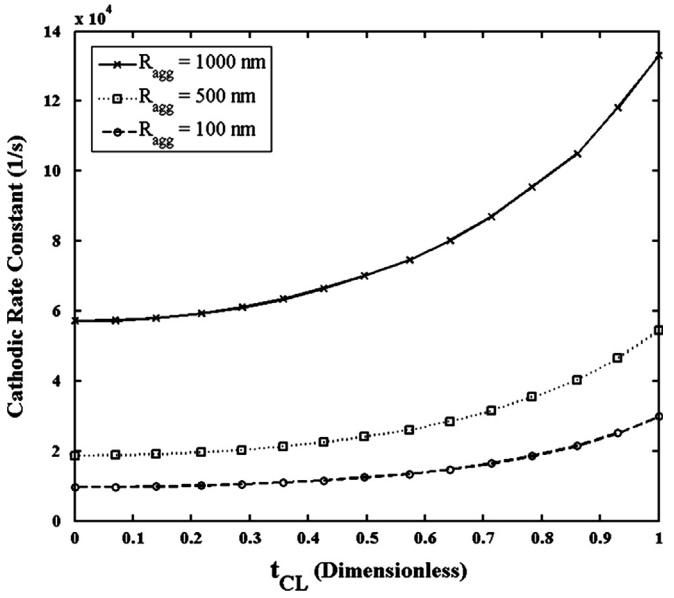

Fig. 10. Local cathodic rate constant profiles for varying agglomerate radius. Here, t_{cl}, m_{Pt}, Pt|C and $\varepsilon_V^{cl}$are held constant at 15 μm, 0.40 mg/cm^2, 0.28, and 0.25, respectively. $V_A = 0.4$ V. $T_{cl} = 0$ corresponds to GDL|CL interface.

Finite element simulations show that the optimum catalyst layer microstructure results in a platinum utilization (kW/g Pt) that is over 30-fold higher than conventional cathode microstructures, while maintaining power densities over 0.35 W/cm^2. The optimized microstructure in this work yields a cathode catalyst layer that produces similar current densities while using only a fraction of the catalyst amount. The effect of increased oxygen transport resistance at low platinum loadings was also included in this study. Inclusion of this added resistance did not significantly alter the optimal design parameters; however, it did reduce the peak platinum utilization and power density to 20.8 kW/g Pt and 0.24 W/cm^2, respectively.

The inclusion of two-phase water flow in the cathode catalyst layer provides this optimization with an additional level of rigor. It was shown that the ultra-low platinum loading microstructure

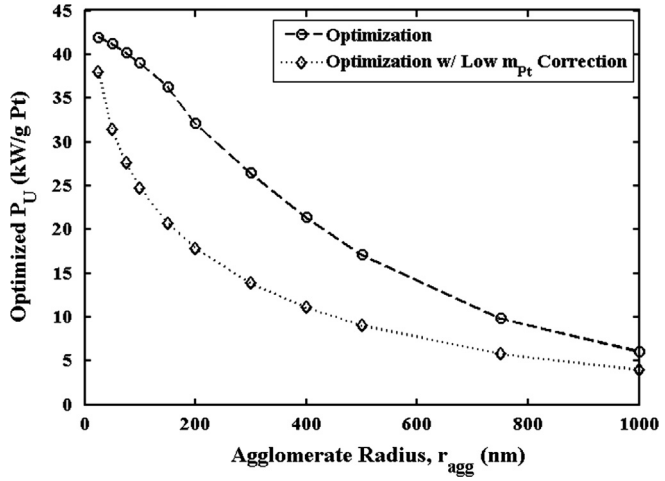

Fig. 11. Effect of agglomerate radius (r_{agg}) on platinum utilization. Results of platinum utilization optimizations at various agglomerate radii are shown. $V_A = 0.4$ V for all simulations; $t_{cl} = 0$ corresponds to GDL|CL interface.

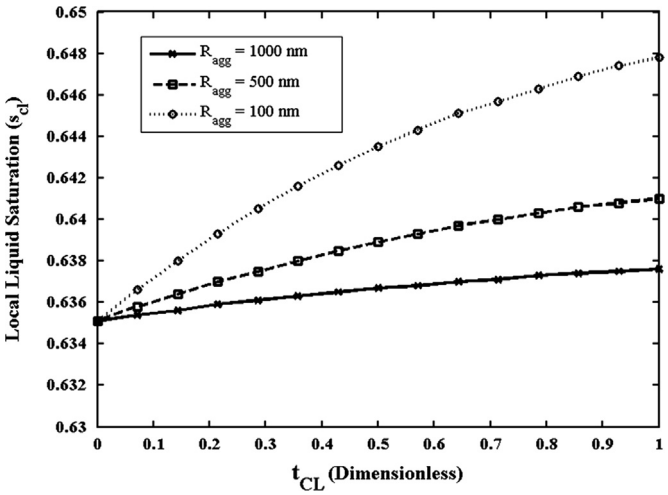

Fig. 12. Effect of agglomerate radius (r_{agg}) on local liquid saturation (s_{cl}) in the cathode catalyst layer. Each curve represents the saturation profile resulting from the microstructure obtained when optimized for maximum platinum utilization at each agglomerate radius. $V_A = 0.4$ V for all simulations, and each catalyst layer is 1.0 μm thick; $t_{cl} = 0$ corresponds to GDL|CL interface.

leads to a very thin catalyst layer that maintains a lower average saturation level when compared with conventional, thicker catalyst layers.

These results are valid for the initial steady state operation of the cell without including the effects of catalyst layer deactivation or membrane degradation. Extended modeling and experimental efforts are underway to validate the model and investigate effects of catalyst deactivation. The results of this work serve to guide the synthesis of high-performance catalyst layers for low-temperature PEM fuel cells.

Nomenclature

English letters

a_r	effective agglomerate surface area, cm^2/cm^3
a_{Pt}	effective catalyst surface area, cm^2/g
a_{Pt}^{agg}	specific catalyst surface area, cm^2/cm^3
C_{O2}^{ref}	reference oxygen concentration, mol/cm^3
C_g	concentration of water vapor in catalyst layer, mol/cm^3

C_{O2}	oxygen concentration in catalyst layer, mol/cm^3
D_c	capillary diffusion coefficient, m^2/s
D_{O2}	bulk oxygen diffusivity, m^2/s
$D_{O2,N}$	oxygen diffusivity in Nafion, m^2/s
D_{O2}^{eff}	effective oxygen diffusivity, m^2/s
F	Faraday's constant, C/mol
$H_{O2,w}$	Henry's constant, atm m^3/mol
i_m	ionic flux, A/cm^2
i_0	exchange current density, A/cm^2
i_0^{ref}	reference exchange current density, A/cm^2
k_c	condensation rate constant, s^{-1}
k_v	evaporation rate constant, s^{-1}
k_t	electrochemical reaction rate constant, s^{-1}
k_N	ionic conductivity, S/cm
K_w	water permeability in catalyst layer, cm^2
m_{Pt}	Platinum loading, (per cm^2 membrane area) mg/cm^2
M_w	molecular weight of water, g/mol
N	electro-osmotic drag coefficient, –
N_i^g	flux of gaseous species in catalyst, layer mol/cm^2 s
N_w	flux of water in catalyst layer, mol/cm^2 s
∇P	capillary pressure, atm
p_{tot}	total operating pressure, atm
Pt|C	mass percentage of platinum catalyst on carbon black, kg Pt/(kg C + kg Pt)
q	switching function, –
R_{agg}	dimensionless agglomerate radius, –
r_{agg}	agglomerate radius, μm
R_{O2}	oxygen reduction reaction rate, mol/m^3 s
R_w	evaporation/condensation reaction rate, mol/m^3 s
t_{cl}	catalyst layer thickness, μm
T_{cl}	dimensionless catalyst layer thickness, –
s	liquid saturation level, –
V_A	applied cell voltage, V
y_v	mole fraction of liquid water, –

Greek letters

α_c	charge transfer coefficient, –
δ_N	Nafion film thickness, μm
δ_W	water film thickness, μm
ε_{agg}	agglomerate ionomer volume fraction m^3 ionomer/m^3 agglomerate
ε_N^{cl}	catalyst layer ionomer phase volume fraction m^3 ionomer/m^3 nanoporous catalyst
ε_S^{cl}	catalyst layers solid phase volume fraction m^3 solids/m^3 nanoporous catalyst
ε_{th}	percolation threshold, –
ε_V^{cl}	catalyst layer void phase volume fraction m^3 nanoporous void space/m^3 nanoporous catalyst
ξ	effectiveness factor, –
μ_w	viscosity of water, cP
ρ_C	platinum density, kg/m^3
ρ_{Pt}	carbon density, kg/m^3
ρ_w	density of water, kg/m^3
Φ	Thiele modulus, –
Φ_m	ionic phase potential, V
τ	tortuosity, –

Superscripts/subscripts

GDL	gas diffusion layer
CCL	cathode catalyst layer
g	gas phase
w	water (liquid)
v	water (vapor)
s	solid phase
N	electrolyte phase
V	void phase

Acknowledgment

The authors wish to thank the National Science Foundation Fuel Cell IGERT at Rensselaer, DGE-0504361 for supporting this work.

References

Bernardi, D., Verbrugge, M.W., 1991. Mathematical-model of a gas-diffusion electrode bonded to a polymer electrolyte. AIChE Journal 37, 1151–1163.
Broka, K., Ekdunge, P., 1997. Modeling the PEM fuel cell cathode. Journal of Applied Electrochemistry 27, 281–289.
Das, P.K., Li, X., Liu, Z.-S., 2010. Effective transport coefficients in PEM fuel cell catalyst and gas diffusion layers: beyond Bruggeman approximation. Applied Energy 87, 2785–2796.
Dobson, P., Lei, C., Navessin, T., Secanell, M., 2012. Characterization of the PEM fuel cell catalyst layer microstructure by nonlinear least-squares parameter estimation. Journal of the Electrochemical Society 159, B514–B523.
Eikerling, M., 2006. Water management in cathode catalyst layers of PEM fuel cells: a structure-based model physical and analytical electrochemistry. Journal of the Electrochemical Society 153, E58–E70.
Evans, J.W., Abbasi, M.H., Sarin, A., 1980. A Monte Carlo simulation of the diffusion of gases in porous solids. Journal of Chemical Physics 72, 2967–2973.
Friedmann, R., Nguyen, T.V., 2010. Optimization of the microstructure of the cathode catalyst layer of a PEMFC for two-phase flow. Journal of the Electrochemical Society 157, B260–B265.
BP Global, 2011. BP Energy Outlook 2030, Washington D.C., April 26th 2011 ⟨http://www.eia.gov/conference/2011/pdf/presentations/Finley.pdf⟩.
Greszler, T.A., Caulk, D., Sinha, P., 2012. The impact of platinum loading on oxygen transport resistance. Journal of the Electrochemical Society 159, F831–F840.
Iszkowski, R.P., Cutlip, M.B., 1980. Voltage losses in fuel cell cathodes. Journal of the Electrochemical Society 127, 1433–1440.
Jain, P., Biegler, L.T., Jhon, M.S., 2008. Optimization of polymer electrolyte fuel cell cathodes. Electrochemical and Solid-State Letters 11, B193–B196.
Jain, P., Biegler, L.T., Jhon, M.S., 2010. Sensitivity of PEFC models to cathode layer microstructure fuel cells and energy conversion. Journal of the Electrochemical Society 157, B1222–B1229.
James B., Kalinoski J., 2009. DOE H_2 Program Review.
Kjelstrup, S., Coppens, M.-O., Pharoah, J.G., Pfeifer, P., 2010. Nature-inspired energy- and material-efficient design of a polymer electrolyte membrane fuel cell. Energy & Fuels 24, 5097–5108.
Lin, G., He, W., Nguyen, T.V., 2004. Modeling liquid water effects in the gas diffusion and catalyst layers of the cathode of a PEM fuel cell. Journal of the Electrochemical Society 151, A1999–A2006.
Litster, S., McLean, G., 2004. PEM fuel cell electrodes. Journal of Power Sources 130, 61–76.
Malek, K., Eikerling, M., Wang, Q., Navessin, T., Liu, Z., 2007. Self-organization in catalyst layers of polymer electrolyte fuel cells. Journal of Physical Chemistry C 111, 13627–13634.
Marr, C., Li, X., 1999. Composition and performance modeling of catalyst layer in a proton exchange membrane fuel cell. Journal of Power Sources 77, 17–27.
Martin, S., Garcia-Ybarra, P.L., Castillo, J.L, 2010. High platinum utilization in ultra-low Pt loaded PEM fuel cell cathodes prepared by electrospraying. International Journal of Hydrogen Energy 35, 10446–10451.
Ono, Y., Mashio, T., Takaichi, S., Ohma, A., Kanesaka, H., Shinohara, K., 2010. The analysis of performance loss with low platinum loaded cathode catalyst layers. ECS Transactions 28, 69–78.
Parthasarathy, A., Srinivasan, S., Appleby, A.J., Martin, C.R., 1992. Electrode kinetics of oxygen reduction at carbon-supported and unsupported platinum microcrystallite/Nafion® interfaces. Journal of Electroanalytical Chemistry 339, 101–121.
Pasaogullari, U., Wang, C.Y., 2004. Liquid water transport in the gas diffusion layer of polymer electrolyte fuel cells. Journal of the Electrochemical Society 151, A399–A406.
Rao, R.M., Bhattacharyya, D., Rengaswamy, R., Choudhury, S.R., 2007. A two-dimensional steady state model including the effect of liquid water for a PEM fuel cell cathode. Journal of Power Sources 173, 375–393.
Sahimi, M., Gavalas, G., Tsotsis, T., 1990. Statistical and continuum models of fluid-solid reactions in porous media. Chemical Engineering Science 45, 1443–1502.
Sakai, K., Sato, K., Mashio, T., Ohma, A., Yamaguchi, K., Shinohara, K., 2009. Analysis of gas transport in catalyst layers; effect of platinum loading. ECS Transactions 25, 1193–1201.
Sander, R., 1999. Compilation of Henry's Law Constants for Inorganic and Organic Species of Potential Importance in Environmental Chemistry. Max-Plank Institute of Chemistry p. 6.

Secanell, M., Karan, K., Suleman, A., Djilali, N., 2007. Multi-variable optimization of PEMFC cathodes using an agglomerate model. Electrochimica Acta 52, 6318–6337.
Secanell M., 2007. Computational Modeling and Optimization of Proton Exchange Membrane Fuel Cells, Doctoral Dissertation, Univ. Victoria, pp. 46–56.
Soboleva, T., Zhao, X., Malek, K., Xie, Z., Navessin, T., Holdcroft, S., 2010. On the micro-, meso-, and macro-porous structure of PEM fuel cell catalyst layers. Applied Materials & Interfaces 2, 375–384.
Soboleva, T., Zhao, X., Malek, K., Xie, Z., Holdcroft, S., 2011. PEMFC catalyst layers: the role of micropores and mesopores on water sorption and fuel cell activity. Applied Materials & Interfaces 3, 1827–1837.
Spendelow J., Martin K. E., Papageorgopoulos D., 2010. Fuel Cell System Cost-2011, DOE Hydrogen and Fuel Cells Record Program. U.S. Department of Energy ⟨http://www.hydrogen.energy.gov/pdfs/11012_fuel_cell_system_cost.pdf⟩.
Sun, W., Peppley, B.A., Karan, K., 2005. An improved two-dimensional agglomerate cathode model to study the influence of catalyst layer structural parameters. Electrochimica Acta 50, 3359–3374.
Wang, X., Nguyen, T.V., 2008. Effects of two-phase transport properties of porous materials on the performance of the cathode of a PEM fuel cell. Journal of the Electrochemical Society 155, B1085–1092.